

ISO 9001 - 2015

ISSN 2349 - 4891

Monthly

IF  
4.665



*Volume 4, Issue 8, August 2017*

International Journal of  
**Recent Research and Applied Studies**

**SURRAGH PUBLICATIONS**  
SURRAGH PUBLICATIONS





## The Structural and Electrical Properties of $(\text{Ni}_{0.25}\text{Cu}_{0.2}\text{Zn}_{0.55}\text{La}_x\text{Fe}_{2-x}\text{O}_4)$ Nano Ferrite

Ahmed R. Abdil Majeed & Rusul A. Najem

Department of Physics, College of Education for Pure Science, Ibn Al-Haitham, University of Baghdad, Iraq.

Received 5th July 2017, Accepted 10th August 2017

### Abstract

Nano ferrite with chemical formula  $(\text{Ni}_{0.25}\text{Cu}_{0.2}\text{Zn}_{0.55}\text{La}_x\text{Fe}_{2-x}\text{O}_4)$ , were synthesized using sol-gel auto – combustion method for the values of  $(X=0.0, 0.025, 0.05 \text{ and } 0.075)$ . The prepared samples were calcined at  $(900^\circ\text{C})$  for  $(2\text{h})$ , The formation of ferrite was confirmed by x-ray diffraction (XRD) and scanning electron microscope (SEM) technique and (EDX). The X-ray diffractometer result shows that ferrite have spinel cubic phase with a particle size ranging from  $(22-29\text{nm})$ , the Lattice constant and density  $(\rho_{x\text{-ray}})$  increased with  $\text{La}^{+3}$  content while the porosity was noticed to decrease. And have been studied dielectric properties It was also observed that the value of the dielectric constant and the dielectric loss factor decreased by increasing the frequency. The increase in alternating conductivity  $(\sigma_{ac})$  was also observed with increasing frequency.

**Keywords:**  $\text{La}^{+3}$  ions, Ferrites; sol -gel method; XRD; SEM; Dielectric Parameters.

© Copy Right, IJRRAS, 2017. All Rights Reserved.

### 1.Introduction

Rare earth materials are known to possess good electrical insulation properties with high electrical resistivity. Therefore, the substitution of these rare earth ions into spinel ferrites could alter the electrical and magnetic properties. Moreover, these rare earth ions have a huge influence on the magnetic anisotropy of the system making the spinel ferrite as promising materials replacing the Hexaferrite or garnets [1,2]. The electrical properties of ferrites are dependent on the microstructure, chemical composition and synthesis technique [3]. Lanthanum is known as the second most abundant and lightest rare earth element (REE) in the lanthanide series. This silvery white mineral found in monazite and bastnasite ores. Lanthanum possesses distinct quality as compared to other REE such as simple electronic spectra which is helpful for experimental analysis; it has the highest boiling point and lowest vapor pressure at its melting point; and at atmospheric pressure lanthanum is the only Superconducting REE [4]. Various methods have been employed in order to synthesize the soft spinel ferrite materials Including chemical coprecipitation [5], hydrothermal method [6], mechano-chemical method [7], micro emulsion method [5], rheological phase reaction method [8], and also sol-gel method [9].

### 2.Experimental Methods

#### A. Materials and Synthesis

The Nano-ferrites of the composition  $(\text{Ni}_{0.25}\text{Cu}_{0.2}\text{Zn}_{0.55}\text{La}_x\text{Fe}_{2-x}\text{O}_4)$  were  $(X=0.0, 0.025, 0.05 \text{ and } 0.075)$  were prepared by using sol-gel auto – combustion method by the below mentioned raw materials. Analytical grade nickel nitrate  $[\text{Ni}(\text{NO}_3)_2 \cdot 6\text{H}_2\text{O}]$ , zinc nitrate  $[\text{Zn}(\text{NO}_3)_2 \cdot 6\text{H}_2\text{O}]$ , copper nitrate  $[\text{Cu}(\text{NO}_3)_2 \cdot 3\text{H}_2\text{O}]$ , iron nitrate  $[\text{Fe}(\text{NO}_3)_3 \cdot 9\text{H}_2\text{O}]$ , citric acid  $[\text{C}_6\text{H}_8\text{O}_7 \cdot \text{H}_2\text{O}]$  and lanthanum nitrate  $[\text{La}(\text{NO}_3)_3]$  were used to prepare  $(\text{Ni}_{0.3}\text{Cu}_{0.20}\text{Zn}_{0.5})\text{La}_x\text{Fe}_{2-x}\text{O}_4$  ferrite with  $x = 0.0, 0.025, 0.050 \text{ and } 0.075$  compositions. Metal nitrates and citric acid were dissolved in deionized water, all these are collected in glass beaker and mixed well at room temperatures by hot plate magnetic stirrers with high speed, Ammonia solution was added slowly the form of drops into the mixed solution to control its pH until reach threats from 7 with continuous rotation. Gradually increase in temperature to reaches of  $80^\circ\text{C}$  to transform it into a gel and then ignited in a self propagating combustion manner to form a fluffy loose powder The as-burnt precursor powder was then calcined at  $900^\circ\text{C}$  for 2 h. The powder was pressed using a die with diameter  $(1.5\text{cm})$  to produce specimens in a pellet shapes. The pressing load used was  $(7\text{ton})$  and the specimens held for 1min under pressure using a hydraulic press of a maximum load  $15 \text{ ton}$ .

#### B. Characterization

The structural characterization of the prepared nano ferrites was performed by X-ray diffraction analysis and Scanning Electron microscopic analysis. XRD analysis confirms the phase formation and SEM analysis

### Correspondence

Rusul Alla

E-mail: omarbila985@gmail.com, Ph. +9194422 60542

reveals the structural morphology. The dielectric properties of the prepared nano ferrites were measured using LCR meter range of 50KHz to 1MHz. Dielectric parameters such as dielectric constant ( $\epsilon'$ ), dielectric loss tangent ( $\tan \delta$ ) were measured using LCR meter.

**3.Results and discussion**

XRD patterns of  $(Ni_{0.25}Cu_{0.20}Zn_{0.55})La_xFe_{2-x}O_4$  Nano crystals, for all the samples with  $x = 0.00, 0.025, 0.050,$  and  $0.075$  are shown in Fig 1. The X-ray diffraction patterns reveal a single phase cubic spinel structure with few traces of secondary phase. Furthermore, the observed diffraction peaks could be assigned to the reflection plane of (111), (220), (311), (400), (422), (511) and (440) which could be indexed to a single-phase Ni-Cu-Zn ferrite Nano crystal. Meanwhile, the peak corresponding to  $2\theta = 32.21$  is attributed to secondary phase at the grain boundaries for  $(\blacktriangledown)$  LaFeO<sub>3</sub> (ICDD PDF #37±1493) except for the cubic spinel phase. The intensity of LaFeO<sub>3</sub> peak has increased with the increase in La<sup>+3</sup> ion concentration. Furthermore, another secondary phase of [10].

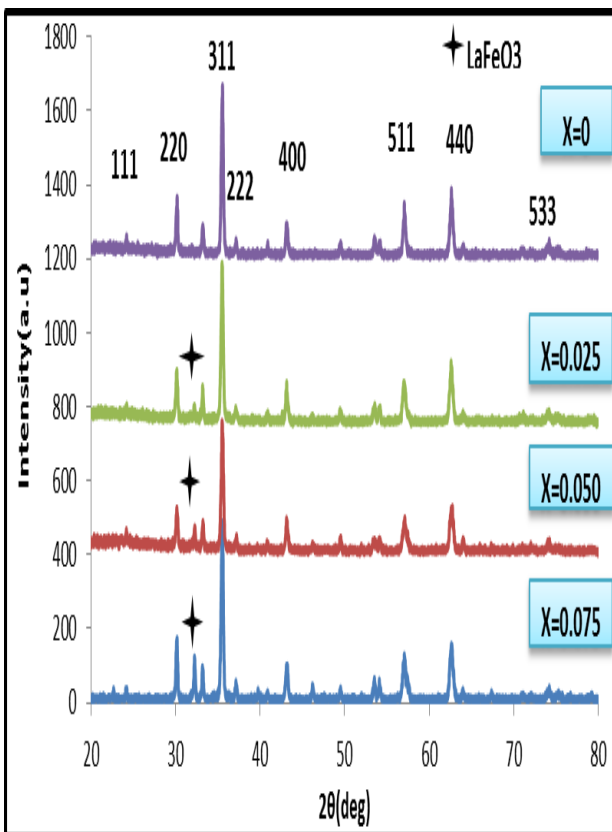


Figure 1 XRD diffraction patterns for the sample of  $Ni_{0.25}Cu_{0.2}Zn_{0.55}La_xFe_{2-x}O_4$

The lattice parameter of individual composition was investigated by using the following relation: [11].

$$d_{hkl} = \frac{a}{\sqrt{h^2 + k^2 + l^2}} \dots \dots \dots (1)$$

Where, 'a' is the lattice constant, d is the interplanar distance and (h, k, l) are the Miller indices

The average crystallite size of the sample is determined using the Scherer's equation [12].

$$D = K\lambda/\beta\cos\theta \dots \dots \dots (2)$$

where D is the crystallite size,  $\beta$  is the full width of the diffraction line at half of the maximum intensity measured in radians,  $\lambda$  is x-ray wavelength (Cu k $\alpha$  radiation, 1.5405Å) and  $\theta$  is the Bragg angle, and Williamson-Hall formula

$$\beta\cos\theta = k\lambda/D_{w-H} + [4\epsilon\sin\theta] \dots \dots (3)$$

The actual (X-ray) density of the samples was calculated using the formula [13],

$$\rho_{x-ray} = \frac{ZM_{wt}}{N_aV} \dots \dots \dots (4)$$

Where M is the molecular weight (Kg) of the sample, N is Avogadro's number (per mol) and a is the lattice parameter (Å). Bulk densities of the samples were determined using the formula,

$$\rho_b = \frac{m}{\pi r^2 h} \dots \dots \dots (5)$$

Where m is the mass (Kg), r is the radius (m) and h is the height of the pellet (m).

Percentage of porosity was calculated using the following formula [14]

$$P = 1 - \frac{\rho}{\rho_{x-ray}} \times 100\% \dots \dots \dots (6)$$

The observed increase in the lattice constant (a) which could be associated with the increasing La<sup>+3</sup> content where the ionic radius of La<sup>+3</sup> (1.6061) is bigger than that of Fe<sup>+3</sup> ion (0.645) replacing iron ions on octahedral B-site which causes asymmetry in the structure. Hence, the lattice constant should be aggrandized with the increasing content of the La<sup>+3</sup> during the substitution process [15, 16] the crystallite size of the samples is observed to increase with lanthanum concentration. This is consistent with the results reported for La<sup>+3</sup>doped Ni-Cu-Zn ferrite [17]. The X-ray density increases linearly with lanthanum ion content and this can be correlated with the increase of atomic weight of La<sup>+3</sup> substituted for Fe<sup>+3</sup> of lower atomic mass. The magnitudes of bulk densities are smaller than that of the corresponding X-ray densities and this difference in magnitude may be attributed to the existence of pores in the bulk samples. The porosity is observed to decrease with La<sup>+3</sup> content.

Table 1  
Effect of La<sup>3+</sup> doping on the lattice parameter, crystallite size, actual (X-ray) density, Bulk density, porosity of (Ni<sub>0.25</sub> Cu<sub>0.20</sub> Zn<sub>0.55</sub>) La<sub>x</sub>Fe<sub>2-x</sub>O<sub>4</sub> system

Sample	X concentrations	Lattice Constant (a)	D <sub>Sh</sub> (nm)	D <sub>w-H</sub> (nm)	ρ <sub>c-ray</sub> (g/cm <sup>3</sup> )	ρ (g/cm <sup>3</sup> )	Porosity %
A <sub>0</sub>	0	8.36	29.70	33.01	5.399	3.50	35.09
A <sub>1</sub>	0.025	8.3775	26.38	31.51	5.43	3.8211	29.72
A <sub>2</sub>	0.050	8.3803	22.28	27.48	5.49	4.05	26.22
A <sub>3</sub>	0.075	8.38	27.46	28.73	5.526	4.09	25.84

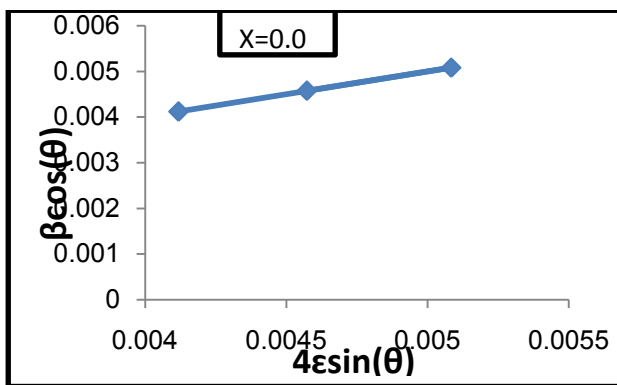


Figure II  
Williamson-Hall plots of (Ni<sub>0.25</sub> Cu<sub>0.20</sub> Zn<sub>0.55</sub>) La<sub>x</sub>Fe<sub>2-x</sub>O<sub>4</sub>

**B. SEM Analysis**

The SEM images of various compositions of NiCuZnLa ferrites were shown in the figure 3. The SEM images reveal that the particles are spherical in shape and are agglomerated in nature. Figure (4) shows the EDX images of all (Ni<sub>0.25</sub> Cu<sub>0.20</sub> Zn<sub>0.55</sub>) La<sub>x</sub>Fe<sub>2-x</sub>O<sub>4</sub> (x = 0.00, 0.025, 0.050, and 0.075) ferrite nanoparticles calcined at 900 °C. The characteristic peaks of Ni, Cu, Zn, La, Fe and O elements were observed in EDX spectra.

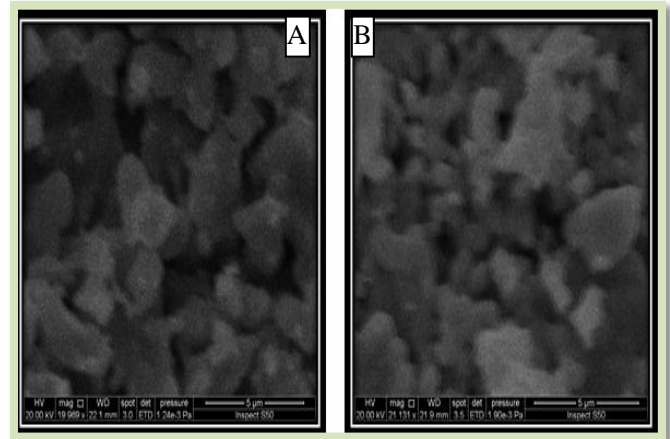


Figure III  
SEM photographs of (Ni<sub>0.25</sub> Cu<sub>0.20</sub> Zn<sub>0.55</sub>) La<sub>x</sub>Fe<sub>2-x</sub>O<sub>4</sub> ferrites with (A) x = 0.00, (B) x = 0.075.

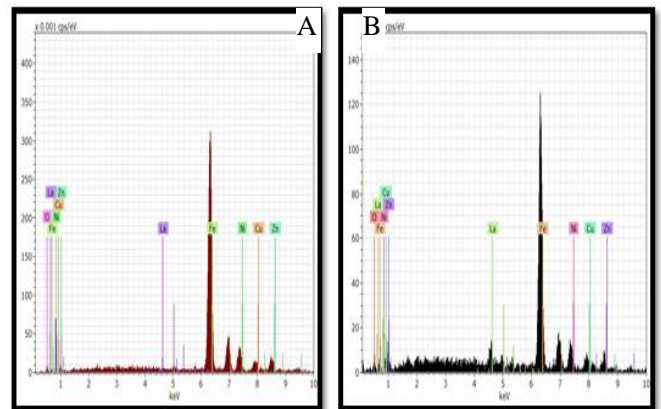


Figure IV  
EDX pattern (Ni<sub>0.25</sub> Cu<sub>0.20</sub> Zn<sub>0.55</sub>) La<sub>x</sub>Fe<sub>2-x</sub>O<sub>4</sub> ferrite nanoparticles with (A) x = 0.00, (B) x = 0.075

**C. Electrical Properties**

The electrical properties of La doped NiCuZn ferrite (Ni<sub>0.25</sub> Cu<sub>0.20</sub> Zn<sub>0.55</sub> Fe<sub>2-x</sub> O<sub>4</sub>), with (X=0.0, 0.025, 0.05 and 0.075) of Lanthanum additions include the a.c conductivity, dielectric properties

**a. Dielectric properties**

The real part of the dielectric constant ε<sub>r</sub>' was calculated by using the relation [18],

$$\epsilon_r' = \frac{Ct}{\epsilon_0 A} \dots \dots \dots (7)$$

Where C is the measured value of capacitance, d is the thickness in centimeters, A is the surface area in square centimeters, ε<sub>0</sub> is dielectric permittivity of air (8.854×10<sup>-14</sup> F/cm). The imaginary part of the dielectric loss ε<sub>r</sub>'' was calculated by using the relation [18],

$$\epsilon_r'' = \tan \delta \epsilon_r' \dots\dots\dots (8)$$

Figures 5 and 6 show the dependence of the real and imaginary part of dielectric constant  $\epsilon_r'$ ,  $\epsilon_r''$ , for bulk  $(\text{Ni}_{0.25} \text{Cu}_{0.20} \text{Zn}_{0.55}) \text{La}_x \text{Fe}_{2-x} \text{O}_4$  on the frequency  $\omega$ , for different lanthanum doping contents. The real and imaginary parts of dielectric constant for all samples decrease with increasing of frequency. This behavior agrees well with Deby's type relaxation process. The real and imaginary parts of dielectric constant reach a constant value for all the samples above certain greater frequency, this agrees with the result of references [19]. It can be observed from Figures 4 that the imaginary parts of dielectric constant  $\epsilon_r''$ , increases with frequency.

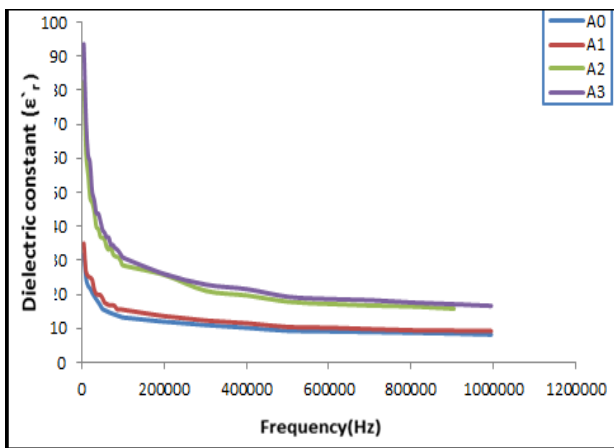


Figure V  
Variation of real part ( $\epsilon_r'$ ) of dielectric constant with frequency for  $(\text{Ni}_{0.25} \text{Cu}_{0.20} \text{Zn}_{0.55}) \text{La}_x \text{Fe}_{2-x} \text{O}_4$  at different La contents

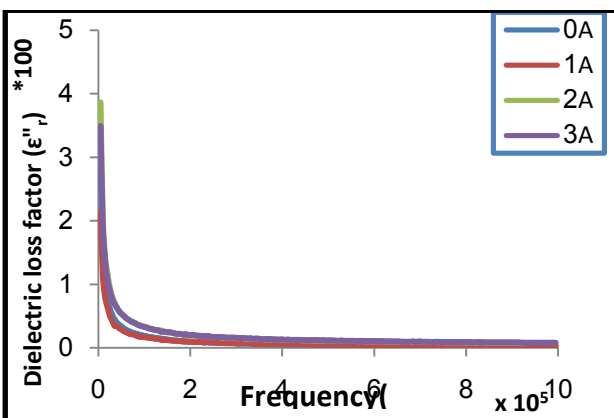


Figure VI  
Variation of imaginary part ( $\epsilon_r''$ ) of dielectric constant with frequency for  $(\text{Ni}_{0.25} \text{Cu}_{0.20} \text{Zn}_{0.55}) \text{La}_x \text{Fe}_{2-x} \text{O}_4$  different La contents

**b. A.C. Conductivity**

The A.C. conductivity was evaluated using the relation [18],

$$\sigma_{(a.c)} = \pi f [\epsilon_r']_0 \epsilon_r' \tan \delta \dots\dots\dots (9)$$

Figure 7 shows the variation of ac conductivity with frequency (50Hz-1MHz). The ac conductivity increases with increasing frequency for all specimens, which is the normal behavior of ferrites this agrees with the result of references [20].

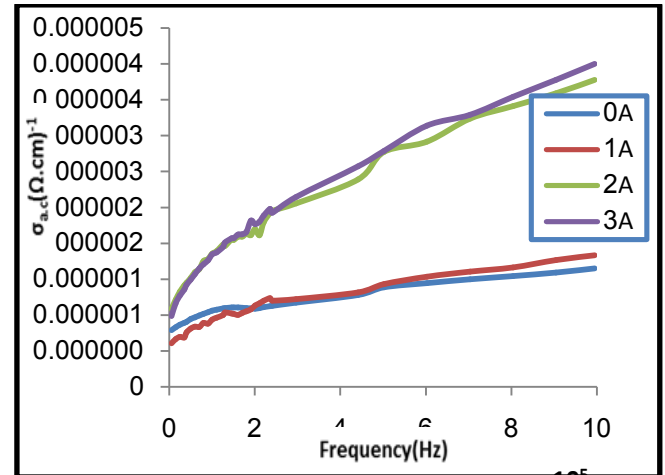


Figure VII  
A.C electrical conductivity as a function of frequency for with  $(\text{Ni}_{0.25} \text{Cu}_{0.20} \text{Zn}_{0.55}) \text{La}_x \text{Fe}_{2-x} \text{O}_4$  different contents of La.

**IV. Conclusions**

The  $(\text{Ni}_{0.25} \text{Cu}_{0.20} \text{Zn}_{0.55}) \text{La}_x \text{Fe}_{2-x} \text{O}_4$  where  $(x = 0.0, 0.025, 0.050 \text{ and } 0.075)$  Nano ferrites were prepared using Sol-Gel method. The X-ray diffraction studies clearly showed formations of the crystalline structure of  $(\text{Ni}_{0.25} \text{Cu}_{0.20} \text{Zn}_{0.55}) \text{La}_x \text{Fe}_{2-x} \text{O}_4$  is cubic spinel structure phase ferrite and The Average crystallite size (D) was calculated as (22-33nm) using Williamson's Hall and Debay shere equation. The lattice parameter is found to increase with increasing lanthanum content. The real and imaginary part of dielectric constant decrease with increasing of frequency, while the A.C electrical conductivity is increased with increasing of frequency.

**References**

1. Shinde TJ, Gadkari AB, Vasambekar PN. Influence of Nd<sup>3+</sup> substitution on structural, electrical and magnetic properties of nanocrystalline nickel ferrites. Journal of Alloys and Compounds. 2012; 513:80± 5.
2. Pervaiz E, Gul I, editors. Influence of rare earth (Gd<sup>3+</sup>) on structural, gigahertz dielectric and magnetic studies of cobalt ferrite. Journal of Physics: Conference Series; 2013: IOP Publishing
3. A. Verma, R. Chatterjee, "Effect of zinc concentration on the structural, electrical and magnetic properties of mixed Mn-Zn and Ni-Zn ferrites synthesized by the citrate precursor technique" J. Magn. Mater. Vol. 306, 2006, PP. 313-320.

4. Krishnamurthy N, Gupta CK. Extractive Metallurgy of Rare Earths: CRC Press; 2004.
5. Dar MA, Shah J, Siddiqui W, Kotnala R. Study of structure and magnetic properties of Ni±Zn ferrite nano-particles synthesized via co-precipitation and reverse micro-emulsion technique. Applied Nano science. 2014; 4(6):675±82.
6. KoÈseoglu Y, Bay M, Tan M, Baykal A, SoÈzeri H, Topkaya R, et al. Magnetic and dielectric properties of Mn<sub>0.2</sub>Ni<sub>0.8</sub>Fe<sub>2</sub>O<sub>4</sub> nanoparticles synthesized by PEG-assisted hydrothermal method. Journal of Nanoparticle Research. 2011;13(5):2235±44.
7. Yang H, Zhang X, Ao W, Qiu G. Formation of NiFe<sub>2</sub>O<sub>4</sub> nanoparticles by mechanochemical reaction. Materials Research Bulletin. 2004; 39(6):833±7.
8. Jing J, Liangchao L, Feng X. Structural analysis and magnetic properties of Gd-doped Li-Ni ferrites prepared using rheological phase reaction method. Journal of Rare Earths. 2007; 25(1):79±83.
9. Hussain A, Abbas T, Niazi SB. Preparation of Ni<sub>1-x</sub>Mn<sub>x</sub>Fe<sub>2</sub>O<sub>4</sub> ferrites by sol gel method and study of their cation distribution. Ceramics International. 2013; 39(2):1221±5.
10. Bugad R, Mane T, Navale B, Thombare J, Babar A, Karche B. Structural, morphological and compositional properties of La<sup>3+</sup> substituted Mg±Zn ferrite interlocked nanoparticles by co-precipitation method, Journal of Materials Science: Materials in Electronics.1±7.
11. Cullity BD. Elements of X-ray Diffraction. California: Addison – Wesley; 1978.
12. Gao F, Qin G, Li Y, Jiang Q, Luo L, Zhao K, et al. One-pot synthesis of La-doped SnO<sub>2</sub> layered nanoarrays with an enhanced gas-sensing performance toward acetone. RSC Advances. 2016; 6(13):10298±310.
13. Sutka A, Mezinskis G, Lulis A. Electric and dielectric properties of nanostructured stoichiometric and excess-iron Ni–Zn ferrites. Phys Scr 2013; 87: 025601 – 7.
14. Aghav PS, Dhage VN, Mane ML, Shengule DR, Dorik RG, Jadhav KM. Effect of aluminum substitution on the structural and magnetic properties of cobalt ferrite synthesized by sol–gel auto combustion process. Phys B 2011; 406: 4350 – 5
15. Wang Y, Xu F, Li L, Liu H, Qiu H, Jiang J. Magnetic properties of La-substituted Ni±Zn±Cr ferrites via rheological phase synthesis. Materials Chemistry and Physics. 2008; 112(3):769±73.
16. Anupama MK, Rudraswamy B. Effect of Gd<sup>3+</sup>Cr<sup>3+</sup> ion substitution on the structural, electrical and magnetic properties of Ni±Zn ferrite nanoparticles. IOP Conference Series: Materials Science and Engineering. 2016; 149(1):012194.
17. Roy, P. K., and J. Bera. "Enhancement of the magnetic properties of Ni–Cu–Zn ferrites with the substitution of a small fraction of lanthanum for iron." Materials research bulletin 42.1 (2007): 77-83.
18. Kambale R C, Adhate N R, Chougule B K and Kolekar Y D 2010 J. Alloys Compd. 491 372 .
19. R. S. Devan, Y .D. Kolekar and B. K. Coagula, "Effect Of Cobalt Substitution on The Properties of Nickel–Copper Ferrite", J. Physics: Condensed Matter, 18, 2006,43.
20. P.A. Noorkhan and S. Kalayne, "Synthesis, Characterization Ac Conductivity of Nickel Ferrite", Journal of Engineering Research and Applications,2, 2012, 681-685.